1-1-2011

Subaerial Freshwater Stromatolites in Deer Cave, Sarawak – A Unique Geobiological Cave Formation

Joyce Lundberg
Carleton University

Donald A. McFarlane
Claremont McKenna College; Pitzer College; Scripps College

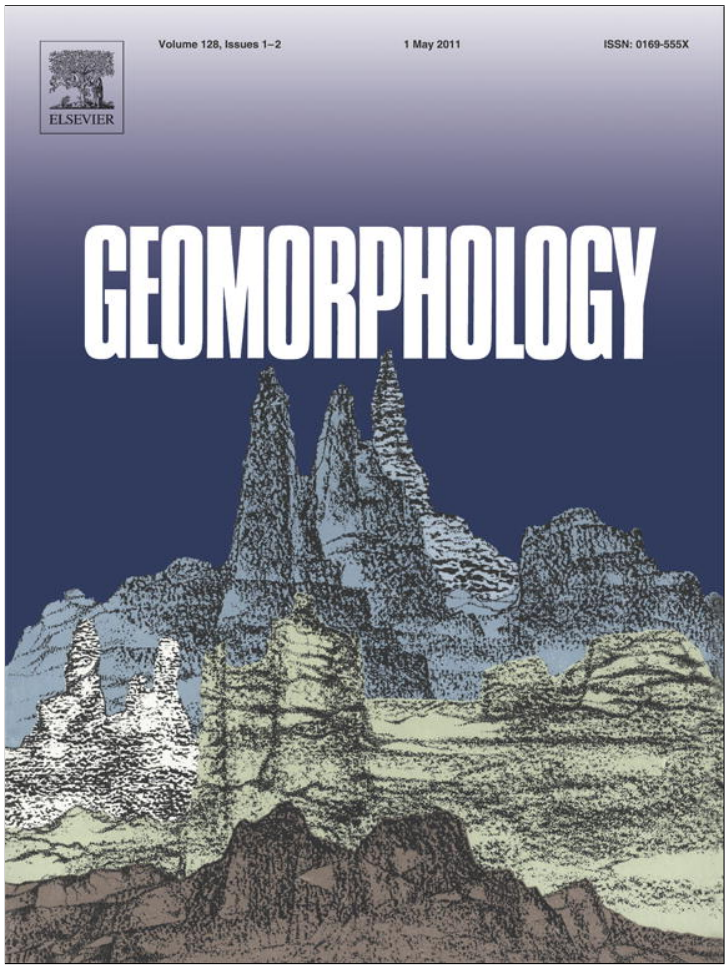

Geomorphology 128 (2011) 57–72

Contents lists available at ScienceDirect

Geomorphology

journal homepage: www.elsevier.com/locate/geomorph

Subaerial freshwater phosphatic stromatolites in Deer Cave, Sarawak — A unique geobiological cave formation

Joyce Lundberg [a,*], Donald A. McFarlane [b]

[a] Department of Geography and Environmental Studies, Carleton University, Ottawa, K1S 5B6, Canada
[b] Wm. Keck Science Center, The Claremont Colleges, 925 North Mills Avenue, Claremont, CA 91711, USA

ARTICLE INFO

Article history:
Received 22 July 2010
Received in revised form 22 December 2010
Accepted 22 December 2010
Available online 4 January 2011

Keywords:
Cave
Subaerial
Stromatolite
Hydroxylapatite
Cyanobacteria
EPS

ABSTRACT

A suite of distinctive freshwater subaerial phosphatic stromatolites is developed close to the northeastern entrance of Deer Cave, Gunung Mulu National Park, Sarawak, Borneo, in conditions of very low light but ample supply of nutrients from guano. These stromatolites are not particulate; they are composed of alternating layers of more porous and more dense amorphous hydroxylapatite. This biomineralization occurs as moulds of coccoid (the majority) and filamentous (less abundant) cyanobacteria. Mineralization occurs at a pH of ~7.0 in the extracellular sheaths and in micro-domains of varying carbonate content in the surrounding mucus of the biofilm. The most recent surfaces that are not yet strongly mineralized show still-living filamentous, coccoid and rod-shaped forms. Trace element composition shows enrichment in metal ions, especially Mn and Zn. The stromatolites are present as horizontal shelves arranged in series on a steep rock face that is vertically under a guano-laden shelf. The rock face undergoes active dissolution from acidic guano drainage water (e.g., pH of 2.43) and from aggressive rainwater from an overhead discharge. However, the rock surface under the stromatolite is protected while the rest of the cliff face is backcut, creating a hoodoo-like effect. The stromatolites are ~15–20 cm deep, ~4–7 cm thick, and of variable width, generally ~50 cm. Eventually, guano and biological detritus in the descending water film lodge in the lee of the stromatolite lip, causing local acidification and erosion of stromatolite and rock on the underside of the ledge. A dynamic equilibrium is established between upward accretion of the fresh surface and destruction at the base such that the base of the stromatolite does not reflect the date of its inception and the stromatolite climbs up the wall.

1. Introduction

Gunung Mulu National Park was designated a World Heritage Site in part because of its potential importance in illuminating processes of biospeleological evolution. Nevertheless, even a basic inventory of the true biodiversity of the caves has barely begun. Here we report on the discovery and characterization of an assemblage of subaerial cave stromatolites unlike any described from anywhere else in the World.

Stromatolites have been defined as laminated organo-sedimentary structures produced by trapping, binding and/or precipitating of mineral matter as a result of metabolic activities of micro-organisms (Seong-Joo et al., 2000). Evidence of microbial participation is required — laminated sediments produced in the absence of organisms as organizing elements and skeletons of encrusting organisms such as coral are excluded. In most stromatolites the currently living tissue is restricted to the uppermost layers, the microbes moving upwards as sediments accrue. The majority of stromatolites are composed of carbonates. The laminated internal structure is the most salient feature, either biological stratification or biomineralogical (Stal, 2000).

Although stromatolites are best known as Precambrian fossils or their living, marine analogs in such places as Hamelin Pool, Western Australia, other habitats are known, including freshwater karstic cenotes in South Africa (Gomes, 1985), Mexico (Gibson, 2006) and south Australia (Thurgate, 1996). In addition, photosynthetic micro-organisms have been implicated in the formation of stromatolitic speleothems in the subaerial photic zone of a few limestone caves. These include the "lobster" or "crayback" structures of the Jenolan Caves, Australia (Cox, 1984), and elsewhere (Gomes, 1985; Cox et al., 1989; Cañaveras et al., 2001). A recent publication by Rossi et al. (2010) documents interesting Mn-rich stromatolites from the interior, non-photic zone of El Soplao Cave, Spain, which are demonstrated to be the product of chemolithotrophic microbes. We agree with Taborõsi (2006), however, in noting that the term "cave stromatolite" has been too widely applied by some authors to include almost any subterranean geomicrobiological structure; here we use the term to apply only to laminar speleothems actively accreted by microbial (here largely cyanobacterial) activity.

Deer Cave (Gua Payou), 4.02 N, 114.82 E, located in Gunung Mulu National Park, Sarawak, Malaysia has been recognized as one of the

* Corresponding author.
E-mail addresses: joyce_lundberg@carleton.ca (J. Lundberg), dmcfarlane@jsd.claremont.edu (D.A. McFarlane).

0169-555X/$ – see front matter © 2010 Elsevier B.V. All rights reserved.
doi:10.1016/j.geomorph.2010.12.022

World's largest cave passages (Brook and Waltham, 1978; Gillieson, 2005), averaging more than 100 m in width, 100 m in height, and extending more than a kilometer through a steep limestone hill. Moreover, the cave has become the centerpiece of tourism at this World Heritage site. In one location close to the "Garden of Eden" (east) entrance to Deer Cave (Fig. 1) the combination of low light and a supply of guano drainage from above has created a fluted rock-face bathed in a continuously flowing film of nutrient-rich water, combined with a sprinkling of fresh water dripping with high kinetic energy from a high ceiling. The unique combination of very low light levels, high nutrient supply, and, most importantly, absence of competition from other photosynthetic organisms has fostered the development of a most unusual group of stromatolitic speleothems (Fig. 2). These cave stromatolites are quite unlike previously-reported examples of cyanobacterial growth in the low-light conditions of cave entrances which results in carbonate deposits such as the lobster/crayback forms. In the Deer Cave stromatolites, forming in a very poorly lit but very wet site, the cyanobacterial mat causes the precipitation of a phosphate (principally hydroxylapatite) matrix.

Gunung Mulu National Park exposes three primary geological formations (Gillieson, 2005; Hutchison, 2005). The basal Setap Shale of Miocene age is overlain by some 2100 m of the very pure, massively bedded Melinau Limestone Formation of Lower Miocene to Upper Eocene age (Wannier, 2009), in which is developed the dramatic tower karst for which Mulu is famous. The highest summits in the Park are composed of Paleocene and Eocene shales and sandstones of the Mulu Formation. Deer Cave cuts through one of the smaller towers in Melinau Limestone, and thus has two large entrances. The north eastern entrance, the site of the stromatolites, opens into the Garden of Eden, one of the world's largest collapse dolines (Gillieson, 2005).

The vegetation around and above the cave is primary evergreen lowland tropical rain forest (Proctor et al., 1983). The climate is governed by the Indo-Australian monsoon system, with the NE monsoon from December to March, the SW monsoon from May to October, and variable winds in the transition periods. The generally high rainfall (4000–5000 mm annually) is mainly from convectional showers each afternoon or evening. The region does not get tropical cyclones. The two peak rainfall periods occur during the transitions between monsoon systems from October to November and April to May. The rest of the year is still relatively wet, July to September being a little less wet. Temperatures in the forest show little variation, either seasonal or diurnal, ranging from minima of 20.6–22.8 °C (at dawn)

Fig. 2. The stromatolites (grey) emergent from the corroded bedrock face (white) with guano-organic slime coatings (black) (the brown leaf is ~12 cm wide). The example marked by the leaf is one of the few that has developed a depression in the stromatolite against the back-wall and shallow undercut in the rock at the base of the back wall.

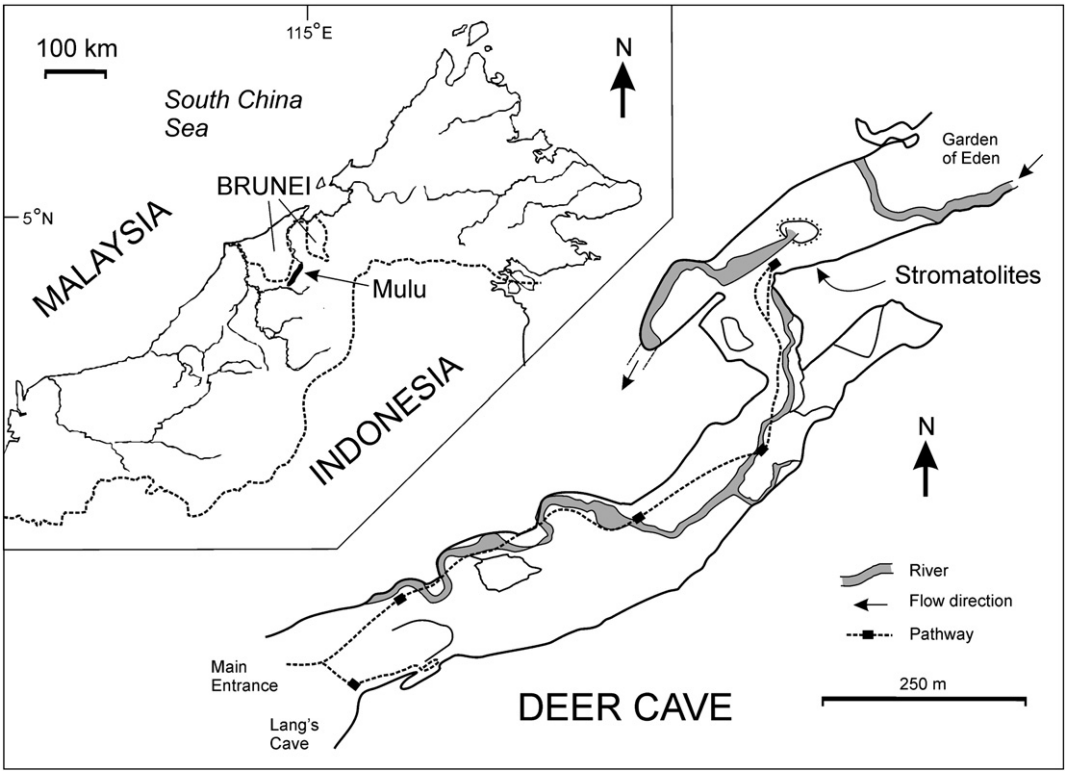

Fig. 1. Location of stromatolites close to Garden of Eden Entrance of Deer Cave. Inset shows location of Mulu in Malaysia (northwest Borneo) close to the border with Brunei. Cave survey based on Brook and Waltham (1978).

up to maxima of 26.7–28.9 °C (in bright sunshine), with typical diurnal ranges of 5.0 °C (Proctor et al., 1983). Mean and maximum temperatures in the Melinau lowlands range from 23 °C to 26 °C (McGinley, 2008).

2. Methods

The location was surveyed in the field (using standard compass and clinometer cave survey techniques) with particular attention to the aspect of the stromatolites with respect to the entrance (the source of light), the situation with respect to the main cave river (potential fluvial erosion), and the sources of inputs (water, guano, and nutrients). Since the site is constantly under a shower of water, and regular small mass movements of guano from the shelf above, the site itself could not be instrumented. A more protected site 6 m away from the wall was instrumented with a HOBO light and temperature logger for 6 days. The logger gives only relative readings and so was calibrated against a light meter (Extech model 401025; resolution 1 lux; accuracy ± 5%; peak response 560 nm). The difference in light levels between the stromatolite site and the logged site was 2 lux (spot readings using the Extech light meter) and the record is adjusted accordingly.

The whole population was documented photographically and a selection measured. The spatial relationships of the large flutes, the guano piles and the stromatolites were surveyed. We looked for similar features in other parts of this cave and in other caves of the region, finding none.

In-situ tests of pH were done using an Extech pH meter: "ExStik" PH100; resolution 0.01, accuracy ± 0.01 pH units, calibrated by 3 points (pH 4, 7, 10) in lab prior to departure, and 1 point on-site (pH 7). Tests were done for pH on the guano piles, and on water films flowing from the guano, over the bare rock, and over the stromatolite surfaces.

A small sample collected under permit was sectioned normal to growth and polished to 1 μm grade. Smaller pieces were studied by Scanning Electron Microscopy (SEM) and Energy Dispersive Spectral (EDS) analysis using a Tescan Vega II XMU machine (Carleton University).

A sample was analyzed for major (SiO_2, TiO_2, Al_2O_3, Fe_2O_3, MnO, MgO, CaO, Na_2O, K_2O, and P_2O_5) and minor (Ba, Ce, Co, Cr, Ga, La, Nb, Nd, Ni, Pb, Rb, Sr, Th, U, V, Y, Zn and Zr) elements and Loss On Ignition (LOI) by X-Ray Diffraction (XRD) and X-Ray Fluorescence (XRF) at the University of Ottawa. The XRD analysis was performed on a Philips 3020 X'Pert system, the samples prepared as a packed powder. The XRF analysis was performed on a Philips PW2400 sequential wavelength-dispersive X-ray fluorescence spectrometer, the samples prepared as fused disks of 4 g of flux (mixture of lithium borates) and 1 g of sample. Another sample was analyzed for trace element composition by inductively coupled plasma mass spectrometric (ICP-MS) analysis at ActLabs, Ancaster, Ontario (51 elements, the Ultratrace 4 package). The acid digested sample was analyzed by Perkin Elmer Sciex ELAN 6000, 6100 or 9000 ICP/MS. The detection limit for most elements is 0.1 ppm.

A 30 μm thin-section was prepared for petrological study at Carleton University and imaged in plane polarized light.

3. Results

3.1. Environmental parameters

The stromatolites are situated at the very edge of the zone of entrance light penetration. The light and temperature data logged over the 6-day period from 27th July to 2nd August 2008 (Fig. 3), show that daytime light levels at the stromatolites can be quite variable depending on cloud cover, reaching a maximum of 6 lux. On the cloudy days light levels averaged only 0.9 lux from 10 am until 2 pm, peaking at 2.0 lux. On sunnier days, the noon to 2 pm average was 2.7 lux, peaking at 5.5 lux. The 6-day average was 0.52 lux. (For comparison typical full moonlight overhead is 0.27 lux: Schlyter, 2006.) The average duration of light on the site was 6.5 hours per day, from 8:10 in the morning until 14:40 in the afternoon.

Temperatures are more variable than is normal inside caves, with the site being close to the huge (200 m diameter) entrance, but still never peaked above 24.2 °C. On clear nights temperatures dropped to 20.8 °C, and on cloudy nights to 21.8 °C. Sharp rises in temperature correlate with sharp rises in light levels. The frequent sharp changes in light levels are caused by passage of storm clouds.

3.2. Distribution and in-field features of the stromatolites

These features (Fig. 2) have been found only in this one location in Deer Cave, and in no other cave that we explored of the Mulu region. The location (Fig. 1) is on the southern wall ~200 m inside the Garden of Eden entrance to Deer Cave. The base of the stromatolites is at ~2 m above normal river level and ~50 m from the main river channel. The sheer size of the passage cross-section limits water levels in all but the most severe flood events. Even the lowermost stromatolites are probably never impacted directly by any flood waters, but may be partly submerged by quiet backwaters during flood events.

Their position in relation to the larger-scale cave wall morphology is important. The main body of stromatolites is developed in the lowermost 4–5 m of a 14-m-high rock face (Fig. 4A, to the left of the person, marked "S"). At the cliff top is a steeply sloping (~35°) bed of bat guano (marked "G" in Fig. 4A) the source of a steady supply of organic-rich water and particles of organic matter that tend to lodge on the rock face. This is also the source of occasional mass movements of guano into the cliff-foot lake (every few hours on wet days). The steepest part of the rock face, to the right of the stromatolites and to a lesser extent above the stromatolites, is deeply eroded by dramatic mega-flutes (marked "F" on Fig. 4A). These are continuously bathed

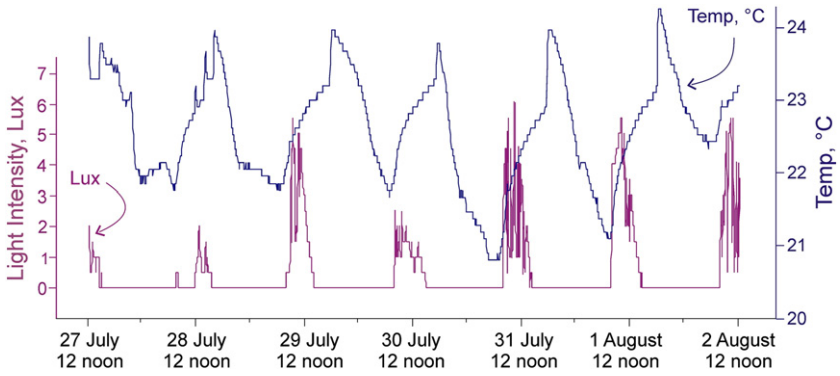

Fig. 3. Light and temperature log (adjusted to reflect levels at the stromatolite site) from 27th July to 2nd August.

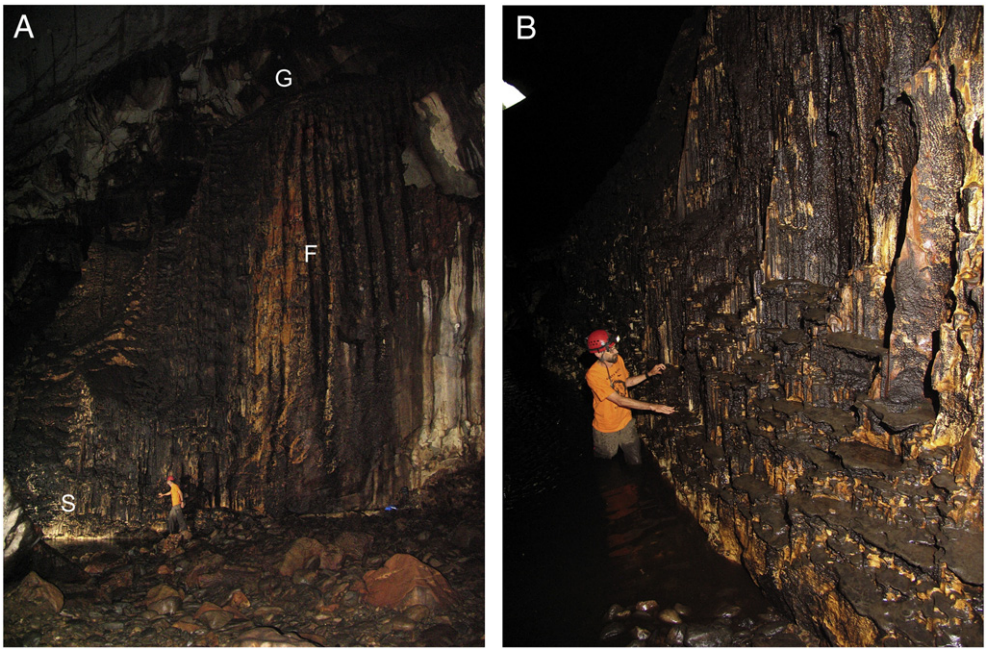

Fig. 4. A. fluted rock face (marked F) above and to the right hand side of the stromatolites. The massive deposit of guano (marked G) that lies on top of the shelf at the top of the flutes cannot be seen in this image. The main body of stromatolites (marked S) is to the left of the person. This is also the location of the showerhead (not strongly discharging when these photographs were taken). B. The person is in the pool of fetid, organic-rich water that is underneath the showerhead and into which regular loads of guano slough from the higher slopes. The main body of stromatolites extends from the foreground to ~8 m behind the person (this view is just to the left of the white S in A). The Garden of Eden entrance is just visible in the upper left side of the photograph (Photographs by Keith Christenson, used with permission).

by drainage water from the guano — so they are essentially huge decantation flutes (Ford and Lundberg, 1987; Lundberg, in press). The site of stromatolite development has the steady supply of guano drainage water, but in addition it is directly underneath one of the showerheads that are typical of this cave. A showerhead is a hollow inverted-funnel-shaped stalactitic speleothem, ~1 m wide, that supplies a constant shower of water from the surface, the discharge varying with precipitation (Hill and Forti, 1997, p. 99). The roof height here (and also the approximate height of the showerhead) is ~120 m (measured by laser rangefinder). Thus the stromatolites are supplied with both the organic-rich water that trickles down the face maintaining contact with the rock face by surface tension, and the showerhead water that delivers rainwater drops at high kinetic energy that wash away some of the organic material but also cause erosion of the rock face.

In the field the stromatolites present as grey slimy shelf-like features emergent from the contrasting white rock face (or pale yellow from surface staining), each occupying the top of a step in the rock face (Fig. 4B). They compose the step part and the bare rock face composes the riser/back wall. Most of them are emergent beyond the front of the step by some 2–5 cm (but can be up to ~10 cm) and this front curls downwards smoothly over the edge. The stromatolite-covered step cuts back into the face up to ~40 cm (the largest one we measured), but the majority are about 15–20 cm deep, while the newly developing ones are very small, barely-identifiable grey patches perched on an irregularity of the rock face. The thickness of the stromatolitic cover can be measured only on the protruding edge and in those cases where rock fall from above has broken off a sizeable part exposing a section. Most of them are 4–7 cm thick and the largest was 13 cm. The horizontal stromatolite shelf can be quite long and continuous, but usually each step has a limited horizontal extent, the small ones only ~10 cm wide and the longer ones ~50 cm, the back having a slightly arcuate form in plain view.

The size varies according to location: the largest forms, of lower frequency (where the person stands in Fig. 4A), are those not so constantly in the pathway of both the showerhead water (which shifts as the wind blows and with discharge) and the falls of rock and guano. This is largely because in the zone where destruction is more likely, the forms do not get the chance to develop without disturbance, and tend to be smaller with higher frequency (beside the person in Fig. 4B).

The top surface of the stromatolite has a thin covering of organic/bacterial slime; the sides and undersides are completely obscured by dark black/brown slime at least 0.5 cm thick. This hangs in dripping streams underneath the shelf and harbours a rich collection of insect remains, and webs (Fig. 5A). In the wet season they are almost constantly under a stream of dripping water. In the (not very) dry season they may not get a constant stream of water but they do not dry out fully, being protected by the mucilage.

The top surface is almost horizontal, sloping gently down towards the front, allowing water to drain freely. Some of the larger forms have a shallow depression on the inner side. This forms when the shelf gets too wide for free drainage. The standing water collects organic matter and the top of the stromatolite begins to decay (Fig. 5A). The base of the rock riser receives deflected splash in addition to the normal erosive waters, so it becomes shallowly undercut (Fig. 5B).

The rock surface that makes up the risers shows evidence of the constant competition between the guano drainage water that coats the whole rock in dark brown matter and the showerhead water that washes it clean. The rock gets cleaner in stormy weather and dirtier in dry weather. The face is eroded into rounded vertical flutes by both waters. The trickling water film held to the rock by surface tension tends to produce small transverse ribs (Fig. 5B), whereas the free-falling drops of high kinetic energy tend to produce undecorated flutes. The ribbed rock is more common towards the outer edges of the stromatolite population where the showerhead discharges are a little less frequent. The overall impression of the stepped and fluted rock face is similar to earth pillars or hoodoos where boulders protect underlying softer material from the action of rainwater. Here it is the stromatolite that protects the underlying rock from dissolution.

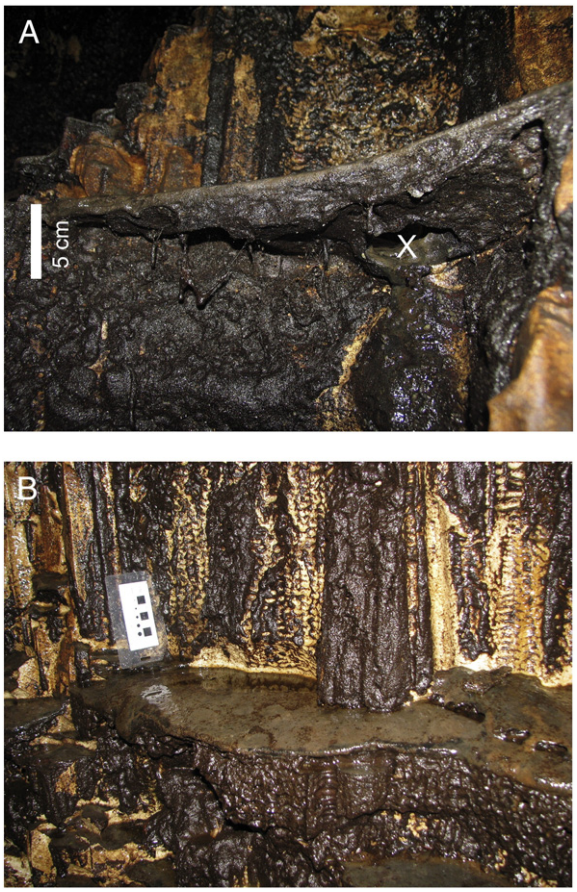

Fig. 5. A. detail of the slime hanging from the underside of the stromatolite shelf. In this example the back of the shelf has eroded through (marked X) (photograph by Keith Christenson, used with permission). B. detail of upper surface and bare rock face. This example has the beginning of a back-wall depression with undercutting, which will eventually break through as in photograph A. The surface film of guano that coats much of the rock face behind the stromatolite is washed away by the showerhead water. In this example the bare rock face is eroded into vertical fluting decorated by delicate transverse ribbing.

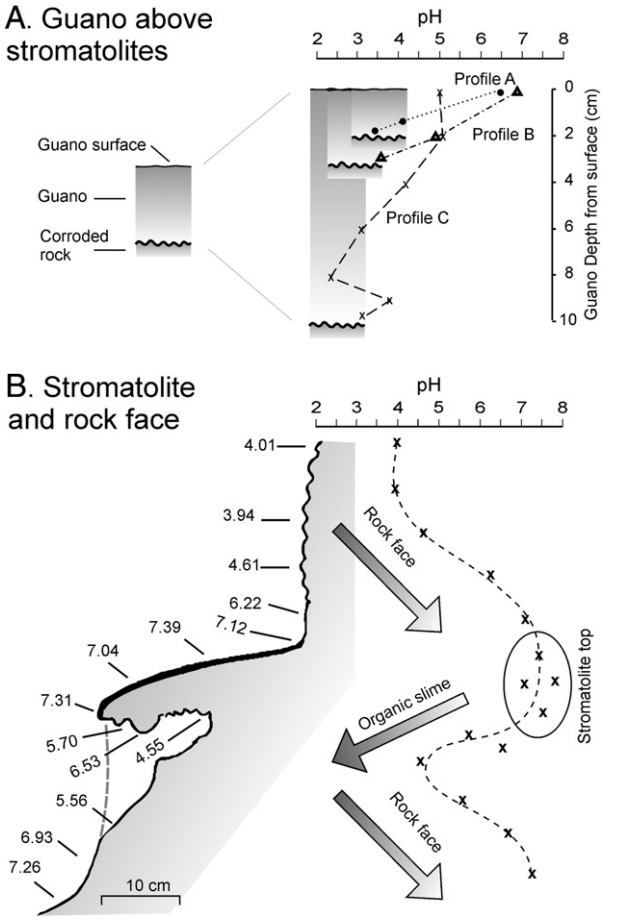

Fig. 6. A: profiles of pH changes with depth in guano above the stromatolites. The three profiles go from the guano surface to the contact with the corroded/crusted rock, each displaying a marked increase in acidity at the base of the guano. B. profile of pH changes down the bare rock riser, the stromatolite top, the sub-stromatolite organic slime, and the next rock riser. The acidic water arriving at the top of the riser rapidly becomes more basic as limestone dissolves (shown by arrow); the stromatolite top remains close to neutral (circled); acidity is renewed in the organic slime, and is once again exhausted by transit across the rock face. In B the dashed line from the stromatolite tip shows the presumed rock profile before being corroded by the acidic slime.

3.3. In-field pH results

Measurements of pH were taken of the wet guano at the top of the cliff, and then of the waters on the rock back walls, the stromatolites, and the organic slime.

The pH of the guano water seems to depend on aeration. When disturbed the guano emits a strong odour of H_2S. A pit dug into deep guano in the slope about 5 m back from the edge of the cliff showed a temperature increase from 25.6 °C at the surface to 30.2 °C at 70 cm depth (suggesting organic activity), and pH values changing from 6.22 at the surface to 8.48 at depth (the absence of acidification here suggests anaerobic respiration). The water that emerges at the edge of the cliff, where the guano is thin and aerated is dramatically acidified. Examples of shallow pits dug into guano here yielded pH values at the surface of 5 to 7, and at the base of 3 to 4, the most acidic value being 2.43 (Fig. 6A). The rock surface here in contact with the guano is softened and altered to at least 2 cm depth.

The stromatolite upper surfaces had pH values close to neutral at 7.08 ± 0.40, as did the shallow pools at their back (7.00 ± 0.46). However, the organic slime underneath the stromatolite ledges was more acidic at 6.26 ± 0.87. Values on the bare rock faces of the risers varied a lot depending on location (6.36 ± 1.21). Fig. 6B shows one profile from the bare rock riser above one stromatolite to the next stromatolite down. The changes in pH tell a clear story: at the top acidified water is supplied from the guano; this causes rock dissolution and becomes more basic downslope; across the stromatolite top pH remains close to neutral; the sub-stromatolitic slime shows a marked augmentation of acidity and distinct corrosion of the rock underneath the stromatolite; the cycle begins again as this acidified water moves down the next riser to the next stromatolite top.

3.4. Anatomy of the stromatolites

3.4.1. Structure at the macro-scale

These stromatolites fit into Kershaw's (1994) classification as "very thin biostromes". The macro-scale morphology is tabular, and the shape of the lamina slightly wrinkled (Walter, 1976, p. 6). The hand specimen is shown in cross-section in Fig. 7A and B shows details of the relatively smooth top surface. Details of the depressions that characterize the front side and underside cannot be seen in the field because of the thick dark mucous covering; the neat semi-circular erosional hollows and intervening cusps were seen clearly only after washing the sample (Fig. 7C). The thickness of the small visor at the front depends on the competition between deposition at

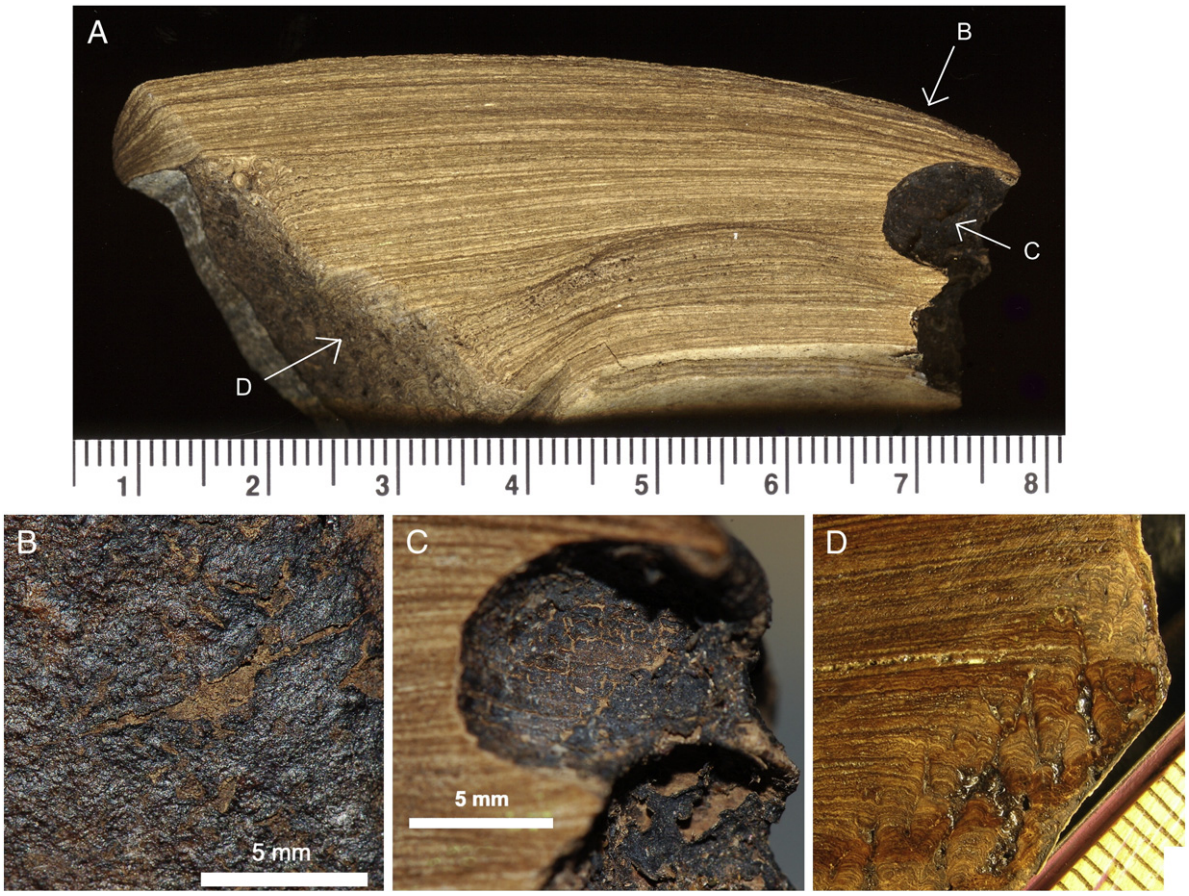

Fig. 7. Lateral view of sample (cut polished face) in approximate growth position. Contact with rock can be seen on the left-hand side. Upper depositional surface was active at time of collection in 2008, and covered with thin layer of bacterial slime. The semicircular bites on the right hand side are erosional, and at the time of collection were obscured by a thick layer of bacterial slime. The bottom of the sample seen in this section is a fracture surface. The unbroken base of the sample also shows circular erosional hollows underneath the slime cover. Scale is in cm. The approximate locations of B, C, and D (taken from other parts of the sample) are shown with white arrows. B: looking down on the upper surface where the organic slime has dried out and cracked. C: detail of the dried cracked organic material coating the erosional hollow. D: detail of the columnar nature of the initial growth at the rock contact (scale in mm).

the top surface and erosion of the side. Similarly the thickness of the whole sample depends on the rate of erosion of the underside. The earliest growth at the rock edge is columnar (Fig. 7D), with the columns coalescing as growth proceeds.

The field evidence shows that the stromatolites occupy the top of a series of back-cutting steps. The hand specimen shows the detail of the step-riser transition. The contact with the rock is not vertical (Fig. 7A) — rather it is at about 60°, indicating that the stromatolite sits on a little rock bevel, in this small example about 1.5 cm wide at the base (an important observation for the modeling of stromatolite genesis, discussed below).

The polished face reveals that the whole sample is built of alternating couplets of white and brown laminae, smooth and continuous at the top but truncated at the eroded edge. Some 70 laminae were counted in this 24-mm-thick sample, with each lamina approximately 0.35 mm thick.

3.4.2. Structure at the micro-scale

The thin sections (Fig. 8) show the laminated, porous nature of the stromatolites. The laminae are usually separated by lines of holes. Each lamina is made of three parts: a pale buff-coloured porous layer; a more dense and lighter coloured layer; and a cap of dark brown organic-rich material. The surface of each lamina is somewhat irregular (Fig. 8B).

Scanning electron microscopy confirms that the laminae are made up of alternating folia of more dense amorphous material separated by more porous horizons (Fig. 9A). At higher magnification (Fig. 9B, C) they can be seen to be composed of an amorphous ground mass infilling the interstices between an intricate network of holes and passages like a miniscule termite mound. Some of these are associated in round clumps (e.g., Fig. 9C). Most of the pores are simply gaps between rounded filament/coccus-mould material (Fig. 9D). In Fig. 9E the form of the hole suggests some stretching of the material to bridge the gap, probably from production of gas bubbles.

Based on the similarity of these forms to published SEM images of modern cyanobacterial mats, these are interpreted to be the moulds of filamentous and coccoid cyanobacteria. In this we follow a well-established precedent: e.g., Kremer and Kazmierczak (2005) appeal to the similarity in the structures of modern cyanobacterial mats to those from Silurian stromatolites to support their argument that the fossil material is likely precipitated by cyanobacterial action; their Fig.3C and D show a modern benthic cyanobacterial mat of coccoid cells embedded in thick mucilage sheaths that appears to be almost identical to our Fig. 9C and F. In another example, Fig. 5E and F from Freytet and Verrecchia (1998) show a colony of filamentous freshwater cyanobacteria encrusted with calcite with a form similar to those in our samples. The clumps in our sample (Fig. 9C) are interpreted as remains of a colonial cyanobacterium with a shared extracellular sheath. Pentecost and Whitton (2000) note that cyanobacteria, such as *Schizothrix*, with bundles of trichomes in a common sheath are abundant in calcareous travertines, especially where prone to emersion. (Note: Some of the channels, such as the

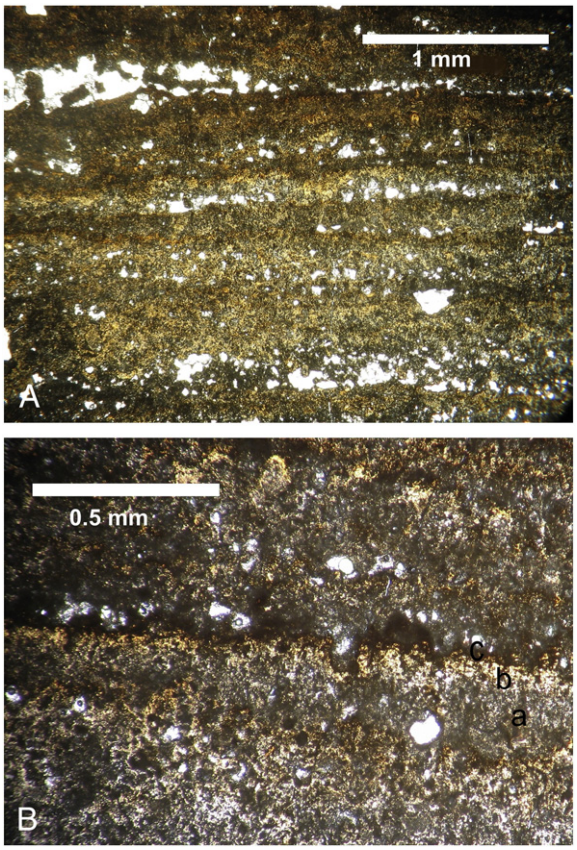

Fig. 8. A: thin section showing laminar nature of material. The lines of holes separate the laminae. B: detail of lamina surface. Although generally quasi-flat, the surface is often irregular at the micro-scale. Each lamina is made up of three layers with gradational boundaries: a pale buff-coloured porous layer (a); a pale-coloured denser layer (b); and a cap of darker brown material (c). The holes are seen to develop above the darkest layer and not all of the laminae have the very clear tri-partite structure.

one shown at the left of Fig. 9C, superficially resemble the burrows carved by endolithic boring fungi/algae; however, in this case they are constructional features.)

Although the number of species apparent here is small, more detailed study reveals some complexities (Fig. 10). The more porous part of the lamina (Fig. 10A) has a greater proportion of the honeycomb structure, more void space and less amorphous groundmass compared to the denser part of the lamina (Fig. 10B). Overall there is a greater proportion of coccoid to filamentous forms and no clear difference in proportions can be seen between the more porous part of the lamina and the more dense part. The coccoid moulds are ~1–2 μm in diameter and the spherical positive forms look like intact mineralized coccoid bacteria (shown in Fig. 10A, B, and E). The filament moulds are generally smaller at ~0.5–1 μm in diameter and some retain plugs of material (Fig. 10B). Where the colonies of coccoid bacteria have not been broken, they present as mammillary shapes (Fig. 10B, C). Also apparent on many of the pore surfaces are rod-shaped bacterial bodies ~0.3 μm in diameter and ~1.4 μm long (Fig. 10D).

The images from the upper surface show the mucilaginous coating dried out and cracked (Fig. 11A), revealing the very porous most recent layer of more solid material, presumed to have deposited during the wet season of 2008 (Fig. 11B). This includes some as-yet-unlithified filaments. An oblique view of the surface under the coating shows filaments emergent from the pores (Fig. 11C). Much of the honeycomb structure here is more translucent to electrons than the older, harder material (and consequently harder to focus on, as can be seen in Fig. 11D). Some unidentified rounded papillary structures ~2 μm in diameter can be seen in Fig. 11D as well as some clusters of rod-shaped bacteria ~1 μm long. The spaces between the honeycomb structures have not been infilled.

The surface underneath the stromatolite also has a mucilaginous coating. Here it is much thicker than the upper one and harbours an interesting collection of debris from the cave, including many insect parts (Fig. 12A) and bat hairs (Fig. 12B). One region shows a concentration of rounded, hollow features (Fig. 12C) attached to the surface by narrow stalks, each ~100 μm tall, ~60 μm wide, with an obvious open mouth ~20 μm wide. These are made up of nanoparticles (Fig. 12D). No EDS was done here; they may well be micritic calcite. These have been tentatively identified as mineralized sheaths of nanoparticles enclosing one of the freshwater saprophagous ciliates of the *Opercularia* sp. (These eat bacteria and suspended sediment, engulfing the food in a funnel-like opening, and are typically 60 to 140 μm tall with short stalks; Sládecek, 1981.) However, Soudry (2000) interprets similar features as envelopes around clusters of coccoid cells.

3.5. Composition of the stromatolites

Chemical composition is indicated by the XRF and ICP-MS results (major and trace elements of homogenized material, Table 1) and EDS results (major elements of surface, Table 2). Carbonate and organic content are indicated indirectly by loss on ignition (LOI). In this limestone cave environment calcium carbonate would be expected to be a major component (44% LOI). However, together with no detectable emission of gas on acid digestion, the low LOI values with the high proportion of phosphate suggest that the Ca is not a carbonate.

The output spectrum from XRD is shown in Fig. 13. The initial short scan-time run suggested an amorphous material, but the main peaks suggested hydroxylapatite $Ca_{10}(PO_4)_6(OH)_2$ (Savarino et al., 1998). Longer XRD scan times confirmed the match with hydroxylapatite. The SEM images indicate that the material is almost totally amorphous, with no clearly crystalline regions, and no material other than amorphous hydroxylapatite is indicated from this XRD analysis. However, EDS mapping shows local regions with higher calcium concentrations, and photographs of polished thick sections (Fig. 7) and thin sections (Fig. 8) show zones within the laminae that are noticeably whiter than the surrounding brown–yellow. This suggests that, while the majority of the material is amorphous hydroxylapatite, local patches of carbonate-hydroxylapatite occur.

Analyses of the major elements by EDS allowed us to compare micro-scale geographic variations in composition (Table 2). The now-cracked mucilaginous coating of the upper surface (column A, Table 2) compared with the most recent layer of stromatolite proper exposed in the cracks (column B) confirmed that the coating is largely made up of C and O, while the stromatolite has the expected C, O, and P of hydroxylapatite. The young layer (column B) is very similar to the older layers (column E). Within the young layer the more dense material (column C) shows a lower C and higher Ca content than the less dense material (column D). In the older material the SEM images sometimes show regions of greater or lesser reflectance of electrons (which relates largely to atomic mass). The dark patches (column F) have higher C, much less P and Ca than the light patches (column G). The geographical distribution of these patches seems to be random.

4. Discussion

4.1. Biological composition

For any structure to be a genuine stromatolite rather than simply a laminated deposit, demonstration of the action of microbes is required. However, there is no consensus on a definition or on how the biogenicity can be demonstrated. Schopf et al. (2007) indicate that

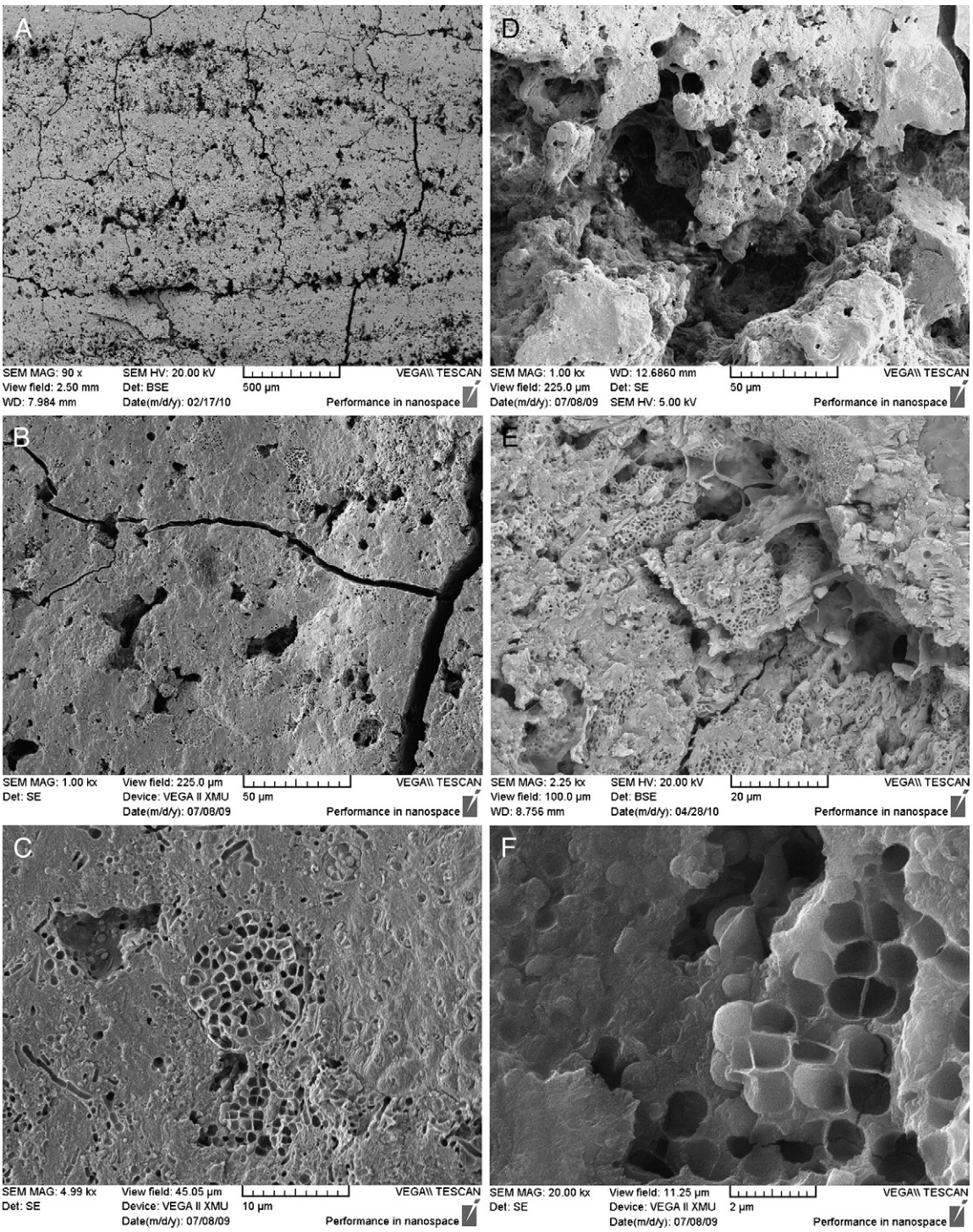

Fig. 9. SEM images. A: the stromatolite in cross-section. The irregular laminae are made up of layers of dense material separated by pores, all of amorphous appearance. (The cracks are artifacts of drying). B and C: at higher magnification the dense network of cavities, each about 1–2 µm in diameter, can be seen. The clump of filaments in C is interpreted as remains of a colonial cyanobacterium with a shared extracellular sheath. In addition to the filament casts ~0.5–1 µm in diameter, the image in C shows many coccoid forms ~1–2 µm in size. D and E: detail of the porous horizon. The rounded forms are themselves made up largely of the lithified cyanobacterial extracellular sheath material. F: close up of one of the (former) cyanobacterial colonies.

definitions vary depending on the focus of the researchers, some emphasizing the biogenic nature and some the sedimentological structure. This disagreement reflects the difficulties in differentiating unambiguously between truly biogenic stromatolites and similar but abiotic deposits, a difficulty exacerbated by the absence or paucity of microfossils in many reported stromatolitic structures. Schopf et al. (2007) remark that, while the simple presence of fossilized microorganisms is not proof of direct causation, the preservation of huge numbers of such fossils comprising the laminae of a stromatolite-like structure would be "exceedingly difficult to understand were such microbes not the formative agents of the structures in which they occur". Schopf et al. (2007) use stromatolite for "accretionary sedimentary structures, commonly thinly layered, megascopic and calcareous, produced by the activities of mat-building communities of

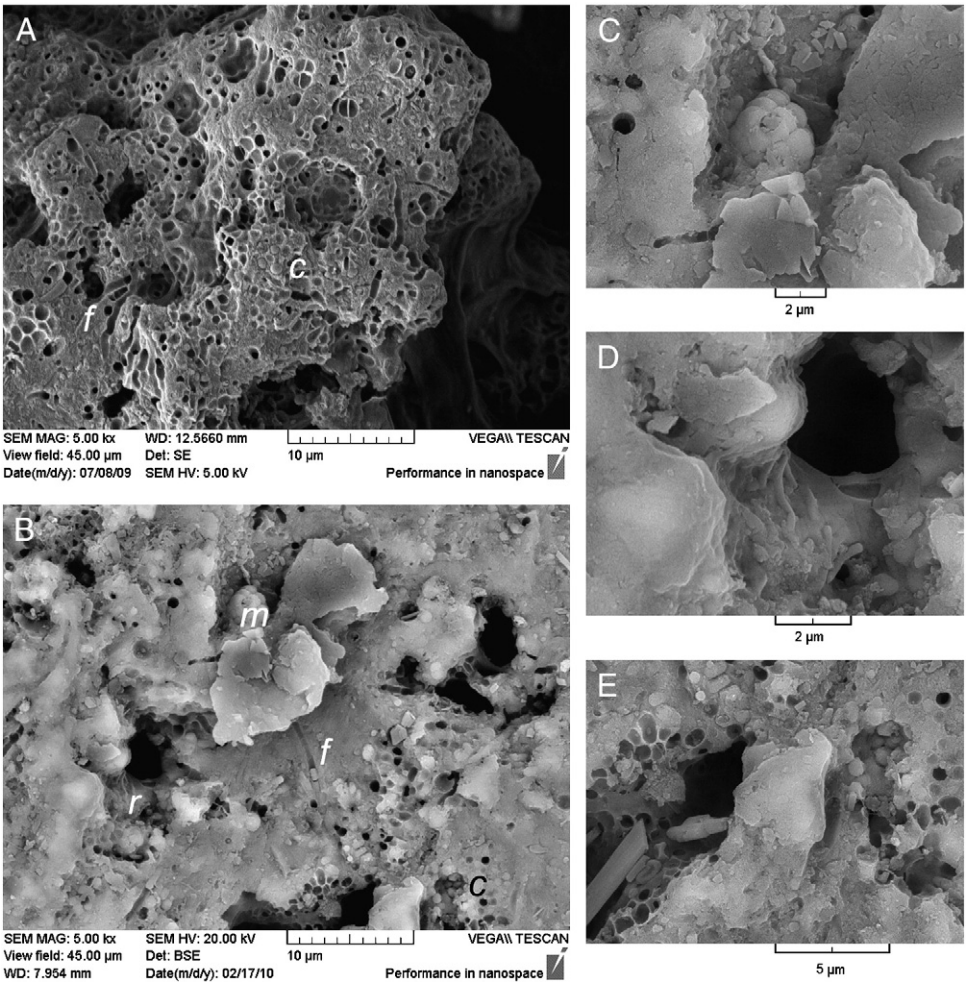

Fig. 10. A: the more porous part of the lamina, composed largely of cyanobacterial fossils and voids. The coccoid forms at "*c*" retain their spherical solid form while the others are moulds. Several show division into two or four cells (e.g., towards the top of this image). Some of the filamentous forms show distinct internal crosswalls, such as that at "*f*". The coccoid forms are generally wider than the filamentous forms. B: the less porous part of the lamina composed of cyanobacterial fossils, amorphous material and only a small proportion of voids (details of this image are shown in C, D, and E). This also shows both coccoid and filamentous forms. The mammillary form (marked as "*m*") is a coccoid colony that has not been broken open. Rod-shaped bacilli can be seen on many surfaces (marked as "*r*"). The filament just beside the "*f*" retains a plug of solid material. C: the mammillary surface of the intact coccoid colony marked as "*m*" in B. A few bacilli can be seen towards the top of this image. D: detail of the rod-shaped bacilli marked as "*r*" in B. E: Detail of the coccoid moulds and intact spherules marked as "*c*" in B.

mucilage-secreting microorganisms, mainly photoautotrophic prokaryotes", while Hofmann (2000) includes under stromatolite any "morphologically circumscribed accretionary growth structure with primary lamination that is, or may be, biogenic", but indicates that ideally they should be both biophoric (containing micro-fossils) and biogenic (microbially influenced). Boston et al. (2001) note that the signature of biological activity includes morphological fossils, mineral-coated filaments, living microbial mats, and preserved biofabrics — all of which are well displayed in the Deer Cave forms. Several species can be seen, coccoid cyanobacteria being the most common, filamentous cyanobacteria the next most common, along with rod-shaped bacteria, and several other rounded forms that are assumed to be bacterial in origin. Traces of the encrusted organisms remain fossilized throughout the deposit and strongly resemble published SEM images of modern bacterial mats (e.g., Freytet and Verrecchia, 1998; O'Brien et al., 2002; Kremer and Kazmierczak, 2005). Many cyanobacteria form bundles of cells within a common sheath (Seong-Joo et al., 2000) — a feature seen throughout our sample.

Another indication of biological activity according to Boston et al. (2001) is the presence of insoluble manganese oxides and oxyhydroxides. Here we see high concentrations of manganese ions (>5000 ppm); the analyses do not tell us the chemical species, but they are likely to be oxides in this aerobic environment.

The mucilaginous material that is produced by many microorganisms is variously termed "extracellular mucilaginous material", "exopolysaccharides", "exopolymer secretions", "biofilm", "mucus", or just "slime" (O'Brien et al., 2002), and usually shortened to "EPS". It is largely by trapping, binding and precipitation of sediment in this EPS that cyanobacterial mats trigger stromatolite growth (Stolz, 2000). This has been found to have a complex structure and house complex chemical reactions and interactions, often with steep chemical gradients. Cell distribution in the biofilm is distinctly clumped with cell-rich zones alternating with exopolymer-rich zones, making a labyrinth of micro-colonies, honeycombed with water channels, and very irregular surfaces (Decko, 2000; Stolz, 2000). Each cell has its own extracellular envelope (or "capsule") but sometimes cells share a common sheath. The thickness of biofilms can be quite variable, typically 1 to 10 mm (Douglas, 2005).

The morphology of the Deer Cave stromatolites – the rounded irregular shapes exposed in the walls of the large pores (e.g., Figs. 9D, and 10A) and making up the surface of the most recent lamina (Fig. 11B), and the uneven surface of organic-rich brown coating apparent in the thin section (Fig. 8B) – suggests that the cyanobacteria are not evenly or randomly distributed; rather they grow in micro-colonies of varying shapes, some bundled filaments sharing a common sheath. These characteristics strongly suggest a biofilm (Fig. 14 shows the biofilm

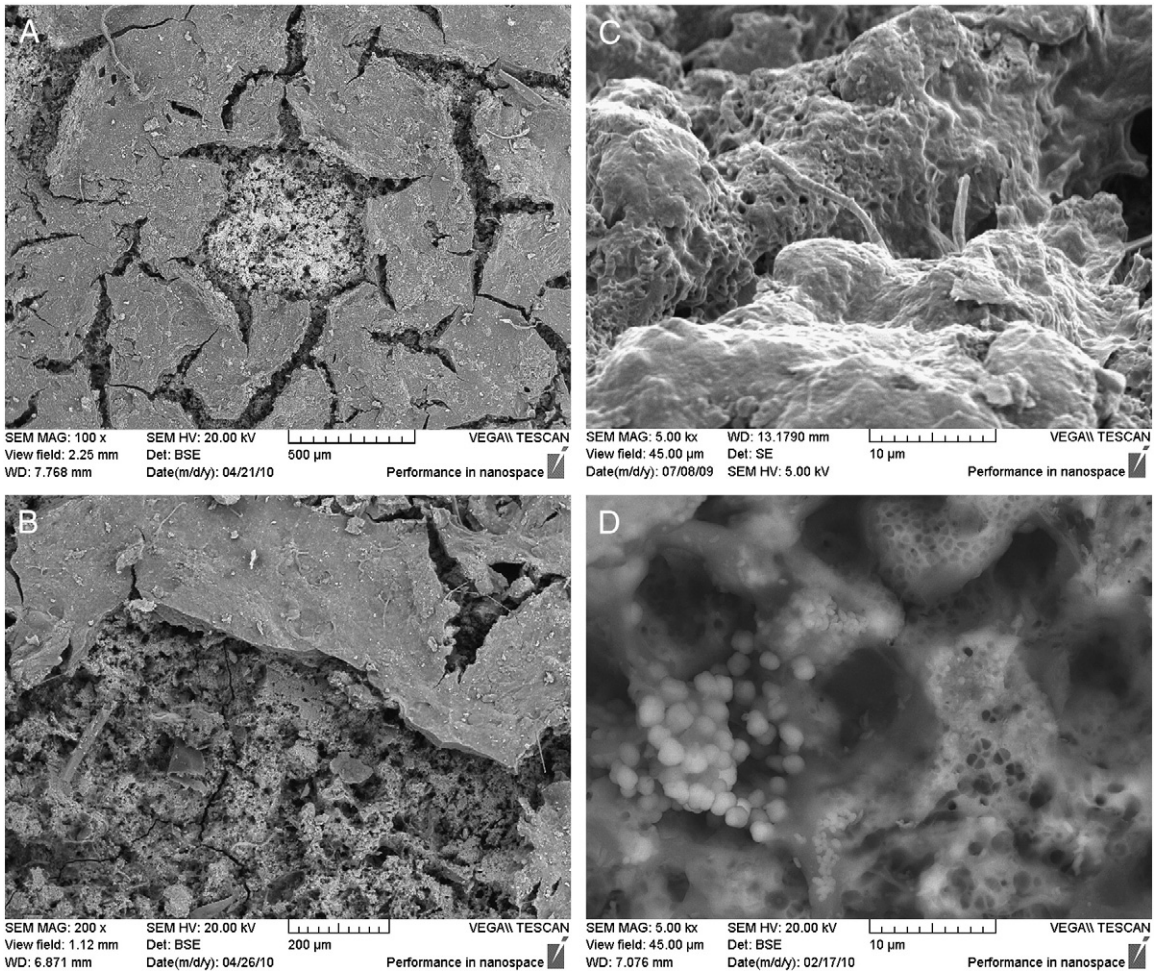

Fig. 11. Features of the young upper surface. A: the mucilaginous cover has dried out and cracked revealing the most recent depositional surface. B: detail of the surface in the crack, showing a very porous texture and a few filaments. C: oblique view of the upper surface under the mucilage with some filaments emergent from the pores. D: detail of the poorly-lithified uppermost surface, with translucent honeycomb structures, ~2 µm spherical features, and clusters of ~1 µm rod-shaped bacteria. This is very similar to many SEM photographs of modern microbial mats, such as Douglas (2005).

diagrammatically). Pentecost and Whitton (2000) note that for some cyanobacteria the colony structure contains calcifying micro-niches. The uneven distribution of ions shown by EDS mapping is also suggestive of the micro-domains of the biofilm. Decko (2000) argues that metals are often chelated and sequestered in micro-domains away from the cells as a protective mechanism to avoid direct exposure of cells to metals.

Classic stromatolitic cyanobacterial mats have a distinct biological zonation (e.g., cyanobacteria in the upper layers, purple bacteria next, green bacteria next; Stal, 2000). No such zonation can be seen in the Deer Cave stromatolites.

4.2. Biomineralization

The process of biomineralization can occur inside the cell, in the extracellular sheath, or in the extracellular matrix (but to be classified as stromatolites, this must not be in the form of skeletal material: Naylor et al., 2002). The effect of biofilms in mediating construction is well documented, especially for carbonates (e.g., Riding and Awramik, 2000). Phototrophic microbes may trigger deposition passively where Ca^{2+} is in good supply simply by their photosynthetic alteration of pH by removal of CO_2 (Cox et al., 1989; Ferris, 2000). Knorre and Krumbein (2000) and Castanier et al. (2000) note that mineralization is increased at high cell densities (and therefore improved if free organic acids are available as carbon source and in eutrophic conditions), at high pHs, and with free gaseous exchange with the atmosphere. In addition the level of biological activity governs the crystal form: they observed a greater proportion of amorphous forms over crystalline forms the higher the nutrient status. All of these conditions apply to the Deer Cave site.

Deposition can be triggered because the cell wall, the sheath, or the EPS act as nucleation sites for mineralization. Douglas (2005) suggests that for bacterial cells nucleation is encouraged by their small size, high surface area to volume ratio and the presence of anionic charge on the cell surface/sheath.

Cyanobacterial mineralization (in those species that do cause mineralization — many do not, even in appropriate chemical conditions) is not simply caused by photosynthesis. Merz-Preiß (2000) notes the importance of the organic macromolecules of the cell sheath. The polysaccharides raise the concentration of divalent metal ions far above the surroundings. In coccoid cells carbonate precipitation in the diffuse slime between cells follows the outline of the cells. Likewise in filamentous cells calcification occurs in the tube around the trichome. Such mineralization can be seen everywhere in the Deer Cave stromatolites.

Most of the literature on biomineralization is about calcification but Soudry (2000) notes that the deposition of phosphates occurs by a very similar mechanism (although all examples are marine and pelagic). It requires a high rate of P supply along with high retention within the uppermost layers of sediment. In well aerated conditions some cyanobacteria sequester polyphosphate in the cell walls (e.g., *Beggiatoa*). In more anoxic conditions, under a filamentous mat, they release the P, which remains in the pore water trapped by the physical barrier of

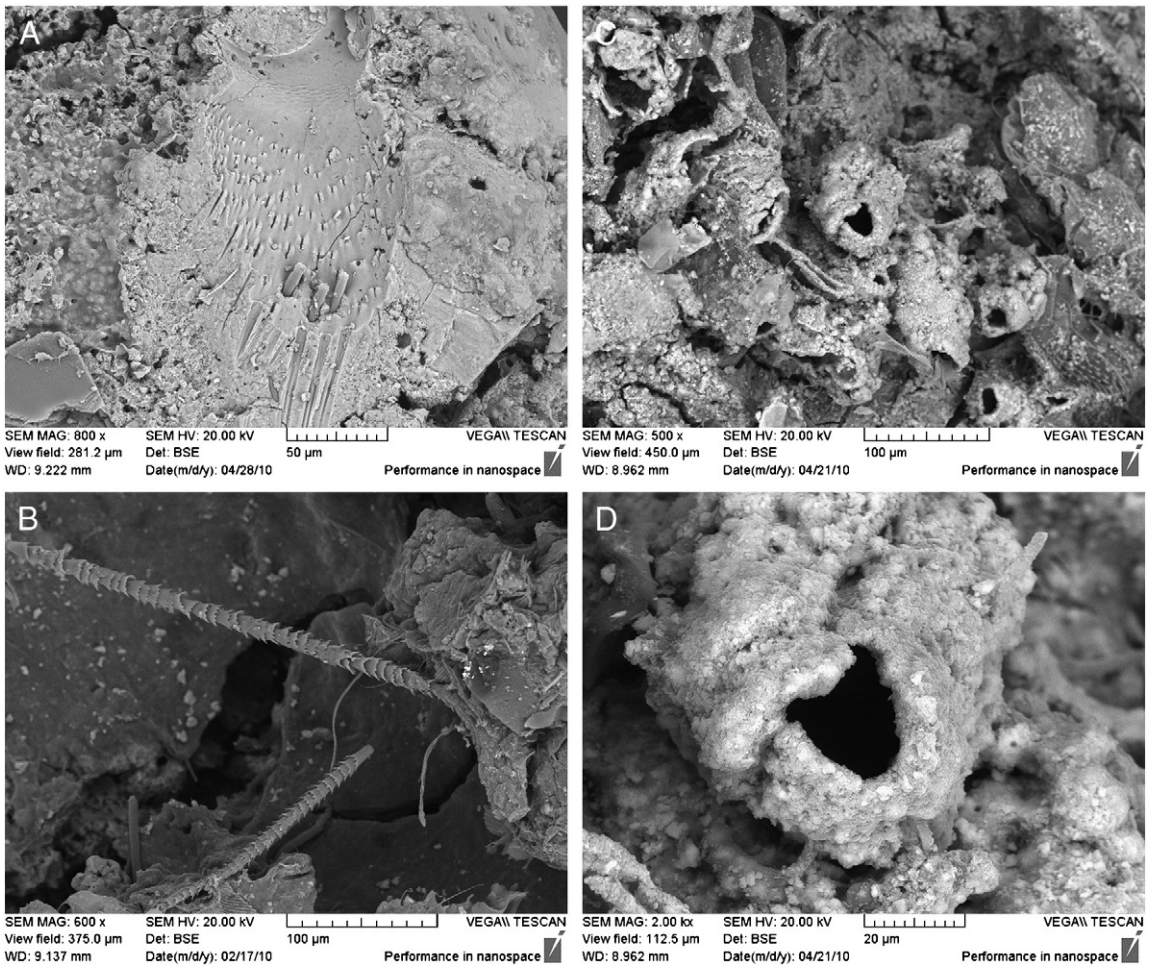

Fig. 12. Features of the underside. A. Remnants of insect entrapped in the mucilaginous slime (possibly antenna of earwig; see photographs in Smith, 2010). B. Bat hair (most likely *Chaerophon plicata*, Wrinkle-Lipped Bat. Hickey and Fenton, 1987). C. Region of funnel-shaped forms tentatively identified as one of the freshwater ciliates *Opercularia* sp. (Sládecek, 1981). D: detail of nanoparticulate composition of the funnel from centre of C.

the organic mat. Crystallization of apatite/phosphate takes place mostly in the extracellular material, and in the intergranular matrix. Mineralisation is probably through a precursor since direct apatite precipitation is kinetically very slow.

Many of the ancient phosphatic stromatolites have become phosphatic only as a result of post-depositional diagenesis but Krajewski et al. (2000) report original phosphatic deposition in some thin (2–4 cm thick) Cretaceous examples. These are nearly pure calcium phosphate, with little detritus, deposited in amorphous or poorly crystalline form. The laminae consist of pure compact apatite and thin porous impure apatite. Some of the original porosity remains (some is infilled with carbonate) and shows abundant moulds of coccoid cells. In some modern phosphorites (non-detrital sedimentary phosphate-rich rocks) mats of filamentous sulphur-oxidising bacteria or of cyanobacteria or of fungus lie directly on the zone of apatite deposition (Rao et al., 2000). Rao et al. (2000) report Pleistocene phosphate stromatolites that formed on the continental shelf off southeast India; these contain both clastic deposits and filament moulds and cell-like structures resembling coccoid cyanobacteria. They suggest that precipitation of amorphous phosphate occurred in some cases in the extracellular matrix soon after the mat organisms died and in other cases intracellularly. Sánchez-Navas and Martin-Algarra (2001) argue, based on the prevalence of features resembling bacterial structures, that the pelagic Upper Jurassic phosphate stromatolites of the Alpine–Mediterranean belt were microbially precipitated. The first stage of precipitation was of amorphous phosphate in association with bacterial mats, in a highly porous texture (and later diagenetically altered).

All the evidence suggests that the stromatolites of Deer Cave are produced, not by trapping of sediment, as in the classic marine stromatolites, but by the precipitation of mineral as a result of metabolic activity of micro-organisms. In our case there is not much evidence for intracellular deposition (most of the moulds remain unfilled), but much evidence of mineralization of the cell walls, the sheaths, and the biofilm. The most recent layer can be seen to be less mineralized than the older layers. The region immediately adjacent to the cells is the first to be mineralized (giving the translucent appearance to the youngest layer); the interstices between the micro-colonies then get infilled.

4.3. Stromatolitic structure

Laminations are the most distinctive feature of stromatolites. The laminae record some oscillation — either of microbial action or of sedimentation (Seong-Joo et al., 2000). Most studies are from marine stromatolites that trap a rain of sedimentary particles; however, the basic causes of laminations may apply in any situation. These include seasonal changes, diurnal changes, storms, solar cycles, and lunar cycles. The mechanism by which the change is expressed in the stromatolite may be microbial behaviour, or by sediment supply, or by changes in microbial composition. In the case of the Deer Cave stromatolites the cause of the lamination is likely to be the balance

Table 1
Elemental composition from XRF analysis and ICP-MS, arranged approximately in descending order of concentration. Concentrations are reported in % or ppm values depending on the sensitivity of the method. Some species are indicated as the oxide (XRF). This table does not include elements at concentrations of less than 1ppm. Not all elements are measured by both methods — e.g, B, S, Cu, Cd, Se are not measured by XRF and Si is not measured by ICP-MS.

XRF			ICP-MS		
Species	%	ppm	Species	%	ppm
L.O.I	23.85				
CaO	41.92		Ca	28.1	
P_2O_5	34.895		P	>10	
MnO	0.707		Mn		5230
			S	0.511	
MgO	0.31		Mg	0.13	1300
SiO_2	0.30				
Zn		1956	Zn		2340
Na_2O	0.18		Na	0.087	
Fe_2O_3(T)	0.132		Fe	0.11	
Al_2O_3	0.06		Al	<0.01	
K_2O	0.018		K	0.02	
Sr		173	Sr		185
TiO2	0.016		Ti	<0.01	
			Cu		116
Ba		75	Ba		87.1
Ni		<10	Ni		10.5
Zr		21	Zr		3.9
V		18	V		9
			B		14
Nd		14	Nd		0.03
Cr		12	Cr		6
			Cd		3.08
Co		<10	Co		2
			Se		1.5
Ce		<10	Ce		1.5

between variation in growth rate of cyanobacteria and variation in water chemistry and hydrology with seasonal changes.

At the micro-scale the Deer Cave stromatolites show the porosity that is, according to Golubic et al. (2000), a characteristic property of organo-sedimentary structures. Some of the pores (or fenestrae — Batchelor et al., 2004) are the spaces formerly occupied by organisms; some are spaces bridged by growing organisms; some are formed by metabolic gases trapped under the microbial mat (e.g., photosynthetically-produced O_2, respiratory CO_2 or anaerobically respired methane — methane production can be considerable and may occur in patches within the biofilm even if the main environment is aerobic: Stolz 2000), and some are left in the lithified structure after decay of the original microbial community (Golubic et al., 2000; Batchelor et al., 2004). The Deer Cave stromatolites have all these types of pore except this last one — there is no evidence for any kind of post-depositional decay within the laminae. The consistency in chemical composition between the most recent layer and the older layers (as shown by EDS analysis) suggests that no post-depositional alteration occurs.

For stromatolites to build up the rate of accretion must be faster than of erosion. For classic detrital stromatolites the uppermost layer

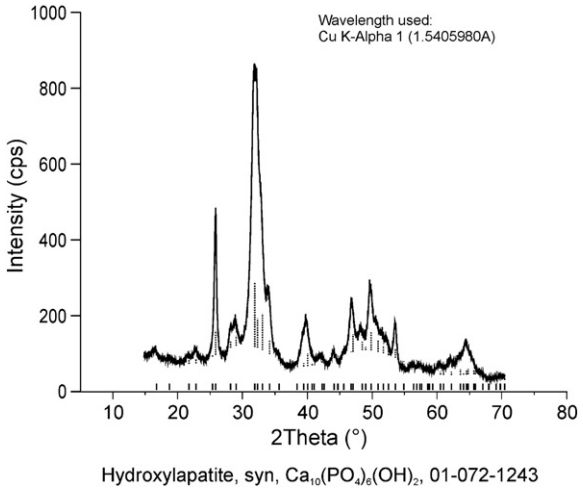

Fig. 13. XRD output spectrum of the material making up the stromatolite.

of living tissue actively calcifies, but decaying organic matter in the underlying layers may shift the chemical balance to erosion. There is a competition between the producers (the cyanobacteria) and the decomposers (bacteria, especially anaerobic respirers, sulphate reducers and methanogens) (Golubic et al., 2000). This does not apply in quite the same way to the Deer Cave stromatolites because the decomposers are not located inside the deposit — rather they accumulate on the outside where the decaying guano-rich slime that collects on the underside causes marked acidification of the water and thus corrodes the outside under-surface. To a small degree there is some decay of the upper surface at the backwall when small pools form at the back of the stromatolite. The third way that they get damaged is because standing a little proud of the rock face makes them susceptible to mechanical destruction as debris falls from above.

4.4. Environmental parameters

We measured light levels at the driest time of the year and thus are likely to have the highest light levels. Even so, several days showed maximum light levels of only 2 lux and sunny days reached only 5.5 lux. These maximum levels are lower than those reported for the other subaerial cave stromatolites, the craybacks/lobsters of Australia (light levels reported as <10 lux; Cox et al., 1989). In addition the average light levels are extremely low since the site is illuminated for only 6 hours each day.

Most of the publications on cyanobacterial growth use an alternative measure of light from lux and thus need to be converted. Energy levels for photosynthetic activity are generally quoted in irradiance units of $\mu E\ m^{-2}\ s^{-1}$. Photometric values are given in lux (lumens per m^2). Conversion between $\mu E\ m^{-2}\ s^{-1}$ and lux is not straightforward because wavelength of energy is required. The

Table 2
EDS results showing atomic percentage values for surface composition of major elements.

Element	A mucus coating (n=6)	B youngest layer of stromatolite (n=6)	C youngest layer, denser texture (n=3)	D youngest layer, open texture (n=3)	E older part of stromatolite (n=6)	F older part, dark patches (n=3)	G older part, light patches (n=3)
C	73.6	36.3	23.2	35.6	40.4	61.5	17.1
O	22.1	42.7	40.4	41.6	44.6	28.2	43.4
P	0.7	7.8	7.6	8.4	6.0	1.4	12.4
Ca	0.8	11.9	26.7	13.1	8.7	2.9	17.3
S	0.8	0.1	0.0	0.0	0.2	1.1	0.0
Mn	0.0	0.2	0.7	0.2	0.4	0.0	0.2

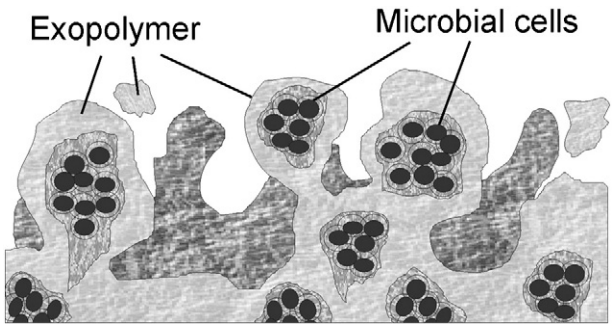

Fig. 14. Diagrammatic view of structure of biofilm (based on Stolz, 2000 and Decko, 2000).

conversion used below for sunlight is: 54 μE m^{-2} s^{-1} = 1 lux (Thimijan and Heins, 1982).

In cyanobacteria, photosynthesis saturates at low light intensities and can continue under very unfavourable light conditions (Stal, 2000). Stolz (2000) observes that the optimum light intensity for cyanobacteria in microbial mats of German North Sea coast is 15–150 μE m^{-2} (*sic*: s^{-1} is assumed) or ~0.3–3 lux. For purple phototrophic bacteria the optimum light is only 5–10 μE m^{-2} or 0.1–0.2 lux. Martinez-Alonso et al. (2004) tabulate light intensities measured in microbial mats from marine environments, the lowest light intensity from a mat in Denmark, at 55 μE m^{-2} s^{-1}, or 1 lux. These values are comparable with the average midday values for the Deer Cave stromatolites on cloudy days (0.9 lux). Thus the stromatolites of Deer Cave are not unique in their tolerance for extremely low light levels.

Temperatures might be expected to show their greatest range on these dry season clear days/nights, but our measurements show nothing remarkable, just a range a little less than that reported by Proctor et al. (1983) for the forest and well within the normal temperature ranges for stromatolites (e.g., those reported by Martinez-Alonso et al., 2004, range from 16 °C to 34 °C).

4.5. Chemical composition

The principal component, hydroxylapatite, is a relatively common material for a cave deposit but unusual for a stromatolite. In most stromatolitic situations phosphorous is limiting, but some cyanobacteria can take up orthophosphate H_3PO_4; this is usually liberated by microbial action but at pH of 7.4–8.1 can change to hydroxylapatite (Stal, 2000). Hill and Forti (1997, p. 118) indicate that hydroxylapatite was first reported in 1882 from caves on Isla de Mona, Puerto Rico. It is one of the four most common phosphate cave minerals. However, it is rare for phosphatic cave minerals to form a distinct morphology. Most are indistinct, fine-grained powders, coatings or crusts within bat guano. Phosphate cave minerals are dissolved and re-precipitated under varying conditions of acidities and cation availability. They are often formed as derivatives from other phosphates. Hydroxylapatite is formed by reaction of phosphoric acid (from bat guano) with calcium carbonate (from rock or sometimes speleothem). The dissolved phosphate ion is precipitated in CO_2-rich water with excess calcium. The acidity of the guano often determines the mineral that will form (Hill and Forti, 1997, p. 163): e.g., carbonate–hydroxylapatite [$Ca_5(PO_4,CO_3)_3(OH)$] forms if pH is greater than 6, while brushite [$(CaHPO_4.2H_2O$] forms at pH below 6. In our case, the field pH measurements of water films suggest that the location of the stromatolites is not random. The pH of the water on the base of the back wall immediately behind the stromatolite and of the stromatolite upper surface was greater than 7, while the waters coming from the guano and from the sub-stromatolite guano-enriched slime were distinctly acidified. This suggests that the stromatolite will form only where the feed waters have picked up enough $CaCO_3$ by rock dissolution to be close to neutral. The acidic sub-stromatolitic slime causes corrosion of the rock that had previously been protected by the presence of the hydroxylapatite coating and corrosion of the stromatolite itself.

The suite of minor elements in the stromatolite is quite distinctive. The Mg and Sr are obviously from the rock. However, the high Mn, Zn, Na, Ti, Cu, Ba, Ni, Zr and V are unusual. Most of these are from the transition metals although Na and Ba are alkali/alkaline-earth metals. Bat guano is one of the likely explanations for the high concentrations, the organic matter, specifically insect chitin, being a potent chelator of metals (Delben and Muzzarelli, 1989; Gamblin et al., 1998, Gyliene et al., 2002). Much of the research on chelation potential of chitin or its derivative chitosan, comes from the study of environmental cleanup, where chitin has been used to extract metal contaminants from waste water. Delben and Muzzarelli (1989) note that chitin has a strong affinity for divalent metal ions. The affinity varies with the metal and with the form of the chitin, but the results reported depend also on the metals of interest to the particular researchers. For example, Delben and Muzzarelli (1989) found for the metals that they studied, that the affinity of chitin decreased from Cu>Cd≫Pb and Ni>Co. In another study, Gyliene et al. (2002) report that the sorption ability of chitin decreases in the order Fe>Cu and Pb>Zn>Ni>Mn and that of chitosan decreases in the rather different order of Cu>Mn>Ni>Zn>Pb>Fe.

Chitin is certainly a part of the deposit, but so are the cyanobacteria that mediate the deposition and the extracellular polymer slime. Cyanobacteria are also known to be effective chelators, secreting siderophores, powerful chelators of iron (Zürcher et al., 2006), copper (Moffett and Brand, 1996), and other metals. Siderophores are produced by both marine and freshwater cyanobacteria (e.g., *Anabaena, Plectonema, Spirulina, Synechoccus, Oscillatoria*: Manahan, 2005, p.70). In addition, extracellular polymers, of which polysaccharide is the major component, are known to concentrate cations, especially divalent metal ions, as well as serve as sites for nucleation (Merz-Preiß, 2000; Lévéille et al., 2007).

The presence in the stromatolites of all three potent chelators (chitin, cyanobacteria and extracellular polymers) offers a very effective mechanism to trap metals and the balance of metal ion concentrations in the stromatolites suggests that all three may be important. The relative concentrations also must vary with supply. One of the more enigmatic is Mn: Hill and Forti (1997, p. 172) mention that phosphate minerals with high Mn have also been found in Niah Great Cave, Borneo, but that the source of Mn has never been identified.

4.6. Comparison with other cave stromatolitic structures

As far as we are aware from the published literature, the subaerial, non-particulate, phosphate stromatolites of Deer Cave are unique, both in their morphology and their composition.

Stromatolites have been reported elsewhere as forming in cave situations but rarely from subaerial settings. For example, Gomes (1985) describes from South Africa 2–3 cm-thick carbonate “tabular crinkled stromatolites” and “columnar-layered stromatolites” that are green/brown in colour, colonized by cyanobacteria, green algae and diatoms, and made of precipitated $CaCO_3$ rather than trapped particles. However, they form on vertical rock faces under water in large open collapse dolines to a depth of ~20 m and can only grow if submerged. Similarly the freshwater stromatolites described by Gibson (2006) are submerged in a well-lit cenote in Mexico, as are the examples of freshwater stromatolites in cenotes of Australia (Thurgate, 1996).

The subaerial cave environment has been shown to host a great variety of micro-organisms, of which many cause corrosion, but some become calcified in situations of super-saturation. The most commonly reported cyanobacteria from cave walls in low light

conditions (admittedly with a bias towards Europe) are *Gloeothece*, and *Leptolyngbya* (Stal, 2000). Some 350 taxa are reported from cave environments although the number of species is greatly reduced in the lowest light levels (Cañaveras et al., 2001; Douglas, 2005; Roldán and Hernández-Mariné, 2009). Jones (2001) notes the many examples of calcite-encrusted cyanobacterial filaments that have been found in caves and on speleothem surfaces. He calls them micro-stromatolites but none of his examples shows a unique landform; all are modifications of normal speleothems, such as micro-columnar accretion around a straw stalactite (see also Baskar et al., 2007; Mulec et al. 2007). Jones (2001) warns that the involvement of microbial action in older deposits may no longer be apparent and thus would go unrecognized. However, there is a danger here of classifying as stromatolitic anything with a finely laminated nature but no overt biological origin.

The hump-backed crayback/lobster forms of some of the Australian caves (e.g., Jenolan and Wombeyan Caves, New South Wales; Cox et al., 1989) are the largest of the reported subaerial cave stromatolites and clearly quite different from the Deer Cave forms. These are metres rather than centimetres in scale, situated in a natural tunnel open at both ends, with relatively high light levels, and open to wind. The laminae consist of smooth calcite (formed during wet seasons) separated by detrital material (accreted during dry seasons by trapping of aeolian sediment). Coccoid cyanobacteria are abundant in superficial layers, but no fossils of cyanobacteria could be found in the deeper layers. It appears that the cyanobacterial extracellular mucilage acts to trap particulate matter, but that the cyanobacteria themselves may not directly cause much precipitation of calcite other than through photosynthetic removal of CO_2.

None of the examples of phosphate deposition in caves reported in the literature appears to be biologically mediated and the review of cave geomicrobiology by Northrup and Lavoie (2001) does not include phosphates in any form. However Forti (2001) does suggest that, although no specific study on the topic has been done, cave phosphates may be at least partially biogenic products. Their composition, environmental situation, and mode of development all suggest that the Deer Cave stromatolites are unique.

4.7. Model of formation

Based on the macro- and micro-morphology and the composition of the stromatolites, the chemistry of the associated waters, and the geomorphology of the rock face, we propose a model to explain the formation of these stromatolites and their relation with the fluted rock face (Fig. 15).

The stromatolites will not form where light levels are high enough for colonization by more complex organisms — so absence of competition is an important criterion that governs location. Also, colonization by these species is unlikely in very acid conditions. Initial colonization by cyanobacteria in patches on the rock face is quasi-random (on any inhomogeneity that catches a little more light). Once a colony has formed the EPS tends to maintain pH close to neutrality (Douglas, 2005). Biomineralization is dependent on a combination of suitable cyanobacterial species, pH approaching 7.0, and an ample supply of Ca^{2+} ions from rock dissolution and phosphate ions from guano.

The obvious question is why the stromatolites should develop into quasi-horizontal ledges. This is most likely a function of the turbulent flow of the water film in combination with an initial inhomogeneity: the bump causes a small hydraulic jump that propagates laterally. Cyanobacterial growth itself and the associated biomineralization then extend the inhomogeneity.

However, the form is also intimately connected with the overall geomorphology of stromatolite and rock. Each encrustation protects the rock beneath it from the fluting erosion that is normal where aggressive waters drip onto, or flow down, a rock face. The rock immediately above is fluted as normal, and the rock surface retreats, leaving behind a small, flat pediment which in turn is colonized by cyanobacteria. Thus the surface expression of the stromatolitic ledge is deeper than the original encrustation that began the process. The rock immediately below the encrustation is fluted only where it is not protected. Since the stromatolites are distributed in patches over some 10 m^2 of cliff face, this process is repeated many times. The resultant form is both visibly and genetically similar to the earth pillars that form where raindrops erode diamictic material — the large fragments are resistant to erosion acting as local capstones to protect the underlying material from the fluting effect of the high-energy raindrops. In Fig. 15 these processes are shown as separate and iterative — in reality they occur simultaneously. The resultant

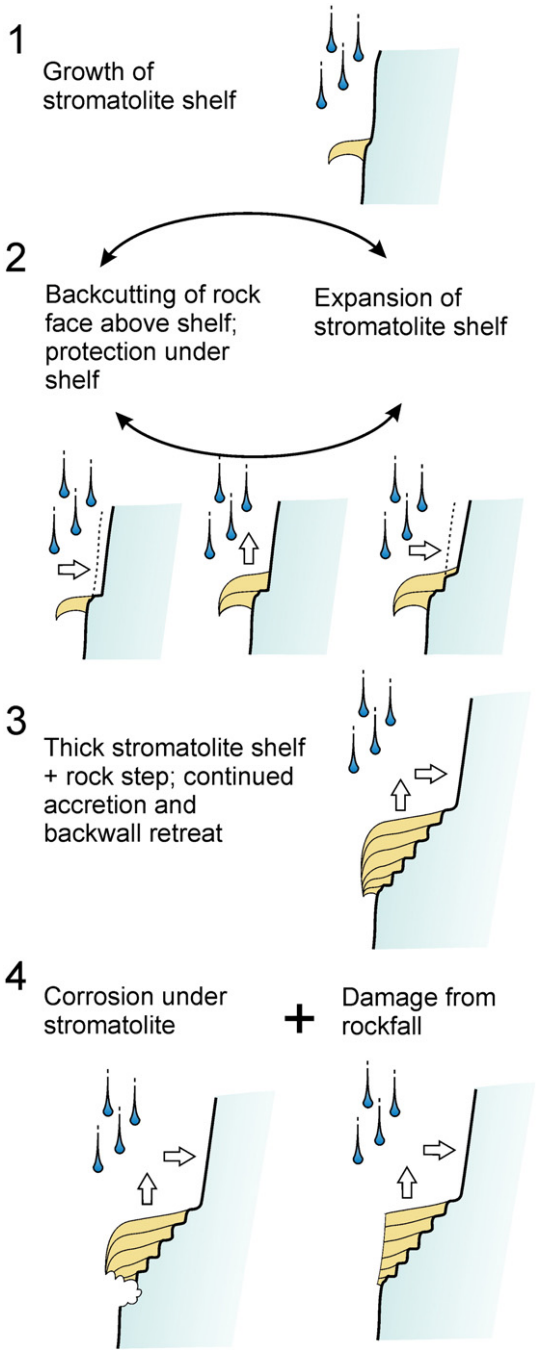

Fig. 15. Model of the development of stromatolites and rock pillars.

stromatolite-rock contact is at an angle as shown but not in discrete steps as shown.

The encrustation cannot widen indefinitely. At least two processes work to limit their width. As soon as they protrude just a little beyond the rock face they are vulnerable to mechanical destruction from falling debris. The other destructive process is an on-going biological corrosion on the sides and undersides from biological activity in the slime that collects under the advancing edge. A dynamic equilibrium develops between the rate of construction and the rate of destruction, inherently limiting the potential longevity of each feature. While construction continues on the upper surface, destruction eats away from the side and underneath, such that the base of any stromatolite is considerably younger than the date of its inception. The stromatolite essentially climbs up the wall.

5. Conclusion

The freshwater subaerial phosphatic stromatolites of Deer Cave represent a rare physical form of the relatively common cave mineral hydroxylapatite. The tropical karst setting provides ample carbonate and ample rainfall. The juxtaposition of dissolving limestone (which raises the pH of the water), guano (which supplies the phosphate), and low light levels (which triggers colonization of cyanobacteria) result in this unusual deposit. Abundant evidence of biological mediation of mineralization is presented in the moulds of coccoid and filamentous cyanobacteria throughout the deposit, along with intact specimens of coccoid, filamentous and rod-shaped forms on recent surfaces. Together with the extracellular biofilm, the relatively constant rainfall keeps the environment damp enough that the cyanobacteria survive the occasional dry episode. The lamination is expressed as a shift in the proportion of pores, mineralized cyanobacterial colonies, and inter-colonial mineralization. We conjecture that this may be controlled by seasonality or by rainstorm frequency, in wetter conditions cyanobacterial growth dominating over inter-colonial mineralization and *vice versa*. This implies that the features may contain a paleoenvironmental record.

This example of phosphatic stromatolites in a subaerial spelean setting appears to be unique. We found no other examples in this cave or in any other caves of the region. The distribution is very much dependent on the particular properties of the site — so it is unlikely that these features are widespread. However, as Jones (2001) notes, research into geological processes mediated by microbes in caves is in its infancy; thus it is probable that other examples of unique structures and processes will be increasingly reported as researchers become more aware of the ubiquity of microbial activity. The fact that these phosphatic stromatolites occur in a sub-aerial freshwater setting rather than a deep marine setting (as appears to be the case for the other phosphatic stromatolites reported in the literature) has implications for interpretation of the fossil record.

Acknowledgements

This work was carried out under Sarawak Forestry Department Permit # NPW.907.4.2(III)-34 and Park permit #24-2008. Funding was provided by a National Geographic Society Research Grant #8437-08, and in part by an NSERC grant to JL. Many thanks to the following: Brian Clark, Syria Lejau and Jenny Malang for in-field support, Keith Christensen for in-cave photography, Tara Kell for XRD and XRF analysis, Mike Jackson for thin section preparation, Jianquin Wang for SEM, and Shelly Hepworth for use of microscope. Thanks to Kurt Konhauser, Robert Riding, and Roger Buick for helpful discussion on an earlier version of this manuscript, and to Jo de Waele and one anonymous reviewer.

References

Baskar, S., Baskar, R., Kaushik, A., 2007. Evidences for microbial involvement in the genesis of speleothem carbonates, Borra Caves, Visakhapatnam, India. Curr. Sci. 92, 350–355.

Batchelor, M.T., Burne, R.V., Henry, B.I., Jackson, M.J., 2004. A case for biotic morphogenesis of coniform stromatolites. Phys. A 337, 319–326.

Boston, P.J., Spilde, M.N., Northup, D.E., Melim, L.A., Soroka, D.S., Kleina, L.G., Lavoie, K.H., Hose, L.D., Mallory, L.M., Dahm, C.N., Crossey, L.J., Schelble, R.T., 2001. Cave biosignature suites: microbes, minerals, and mars. Astrobiology 1, 25–55.

Brook, D.B., Waltham, A.C., 1978. The Limestone Caves of Gunung Mulu National Park. Sarawak. Royal Geographical Society, London. 44 pp.

Cañaveras, J.C., Sanchez-Moral, S., Soler, V., Saiz-Jimenez, C., 2001. Microorganisms and microbial induced fabrics in cave walls. Geomicrobiol. J. 18, 223–240.

Castanier, S., Le Métayer-Levrel, G. and Perthuisot, J.P., 2000. *Bacterial Roles in the precipitation of Carbonate minerals*. In; Riding, R.E., Awramik, S.M. (Eds.), Microbial Sediments, Springer, pp. 32–39.

Cox, G., 1984. Phototropic stalagmites at Jenolan Caves, NSW. Helictite 22, 54–56.

Cox, G., James, J.M., Legget, K.E.A., Osborne, R.A.L., 1989. Cyanobacterially deposited speleothems: subaerial stromatolites. Geomicrobiol. J. 7, 245–252.

Decko, A.W., 2000. *Exopolymer microdomains as a structuring agent for heterogeneity within microbial biofilms.* In; Riding, R.E., and Awramik, S.M. (Eds.), Microbial Sediments, Springer, pp. 9–15.

Delben, F., Muzzarelli, R., 1989. Chitin and its affinity for divalent metal ions. Carbohydr. Polym. 11, 221–232.

Douglas, S., 2005. Mineralogical footprints of microbial life. Am. J. Sci. 305, 505–525.

Ferris, F.G., 2000. Microbe-Metal Interactions in Sediments. In: Riding, R.E., Awramik, S.M. (Eds.), Microbial Sediments, Springe, pp. 121–126.

Ford, D.C., Lundberg, J., 1987. A review of dissolutional rills in limestone and other soluble rocks. In: Bryan, R. (Ed.), Rill Erosion: processes and significance. Catena Suppl. 8, 119–140.

Forti, P., 2001. Biogenic speleothems: an overview. Int. J. Speleol. 30, 39–56.

Freytet, P., Verrecchia, E.P., 1998. Freshwater organisms that build stromatolites: a synopsis of biocrystallization by prokaryotic and eukaryotic algae. Sedimentology 45, 535–563.

Gamblin, B.E., Stevens, J.G., Wilson, K.L., 1998. Structural investigations of chitin and chitosan complexed with iron or tin. Hyperfine Interact. 112, 117–122.

Gibson, M.A., 2006. Preliminary interpretation of a stromatolite field in Laguna Bacalar, Quintannaroo, Mexico. Geol. Soc. Am. Abstr. Programs 38, 25.

Gillieson, D., 2005. *Karst in southeast Asia*. In; Gupta, A. (Ed.), The physical geography of southeast Asia, Oxford University Press, Oxford, pp. 157–176.

Golubic, S., Seong-Joo, L., Browne, K.M., 2000. Cyanobacteria: Architects of Sedimentary Structures. In: Riding, R.E., Awramik, S.M. (Eds.), Microbial Sediments. Springer, pp. 57–67.

Gomes, N.A., de, N.C., 1985. Modern stromatolites in a karst structure from the Malmani subgroup, Transvaal Sequence, South Africa. Trans. Geol. Soc. SA 88, 1–9.

Gyliene, O., Rekertas, R., Salkauskas, M., 2002. Removal of free and complexed heavy-metal ions by sorbents produced from fly (*Musca domestica)* larva shells. Water Res. 36, 4128–4136.

Hickey, M.B.C., Fenton, M.B., 1987. Scent-dispersing hairs (Osmetrichia) in some Pteropodidae and Molossidae (Chiroptera). J. Mammology 68, 381–384.

Hill, C., Forti, P., 1997. Cave minerals of the World, 2nd ed. National Speleological Society, Huntsville. 463pp.

Hofmann, H.J., 2000. Archean Stromatolites as Microbial Archives. In: Riding, R.E., Awramik, S.M. (Eds.), Microbial Sediments. Springer-Verlag, Berlin, pp. 315–327.

Hutchison, E.S., 2005. Geology of North-West Borneo: Sarawak. Brunei and Sabah, Elsevier. 421pp.

Jones, B., 2001. Microbial activity in caves — a geological perspective. Geomicrobiol. J. 18, 345–357.

Kershaw, S., 1994. Classification and geological significance of biostromes. Facies 31, 81–91.

Knorre, H.V., Krumbein, W.E., 2000. In; Riding, R.E., Awramik, S.M. (Eds.), Microbial Sediments, Springer, pp. 25–31.

Krajewski, K.P., Leśniak, P.M., Łącka, B., Zawidzki, P., 2000. Origin of phosphatic stromatolites in the Upper Cretaceous condensed sequence of the Polish Jura Chain. Sed. Geol. 136, 89–112.

Kremer, B., Kazmierczak, J., 2005. Cyanobacterial mats from silurian black radiolarian cherts: phototrophic life at the edge of darkness? J. Sed. Res. 75, 897–906.

Lévéille, R.J., Longstaff, F.J., Fyfe, W.S., 2007. An isotopic and geochemical study of carbonate-clay mineralization in basaltic caves: abiotic versus microbial processes. Geobiology 5, 235–249.

Lundberg, J., in press. *Micro-sculpturing of solutional rocky landforms*. In: Frumkin, A. (Ed.), Karst geomorphology. Treatise on Geomorphology, 6.

Manahan, S.E., 2005. *Environmental chemistry*. 8th Edition. CRC Press, 783 pp.

Martínez-Alonso, M., Mir, J., Gaju, N., Guerrero, R., Esteve, I., 2004. Distribution of phototrophic populations and primary production in a microbial mat from the Ebro Delta, Spain. Int. Microbiol. 7, 19–25.

McGinley, M. (Ed.), 2008. Gunung Mulu National Park, Malaysia. In: Cleveland, C.J. (Ed.), *Encyclopedia of Earth*. (Washington). <http://www.eoearth.org/article/Gunung_Mulu_National_Park,_Malaysia>.

Merz-Preiß, M., 2000. *Calcification in Cyanobacteria*. In; Riding, R.E., Awramik, S.M. (Eds.), Microbial Sediments, Springer, pp. 50-56.

Moffett, J.W., Brand, L.E., 1996. Production of strong, extracellular Cu chelators by marine cyanobacteria in response to Cu stress. Limnol. Oceanogr. 41, 388–395.

Mulec, J., Kosi, G., Vrhovšek, D., 2007. Algae promote growth of stalagmites and stalactites in karst caves (Škocjanske Jame, Slovenia). Carbonates Evaporites 22, 6–9.

Naylor, L.A., Viles, H.A., Carter, N.E.A., 2002. Biogeomorphology revisited: looking towards the future. Geomorphology 47, 3–14.
Northup, D.E., Lavoie, K.H., 2001. Geomicrobiology of caves: a review. Geomicrobiol. J. 18, 199–222.
O'Brien, N.R., Meyer, H.W., Reilly, K., Ross, A.M., Maguire, S., 2002. Microbial taphonomic processes in the fossilization of insects and plants in the late Eocene Florissant Formation, Colorado. Rocky Mt Geol. 37, 1–11.
Pentecost, A., Whitton, B.A., 2000. Limestones. In: Whitton, B.A., Potts, M. (Eds.), The Ecology of Cyanobacteria. Kluwer Academic Publishers, Dordrecht, Netherlands, pp. 257–279.
Proctor, J., Anderson, J.M., Chai, P., Vallack, H.W., 1983. Ecological studies in four contrasting lowland rain forests in Gunung Mulu National Park, Sarawak: I. Forest environment, structure and floristics. J. Ecol. 71, 237–260.
Rao, V.P., Rao, K.M., Raju, D.S.N., 2000. Quaternary phosphorites from the continental margin off Chennai, Southeast India: analogs of ancient phosphate stromatolites. J. Sed. Res. 70, 1197–1209.
Riding, R.E., Awramik, S.M. (Eds.), 2000. Microbial Sediments. Springer. 331 pp.
Roldán, M., Hernández-Mariné, M., 2009. Exploring the secrets of the three-dimensional architecture of phototrophic biofilms in caves. Int. J. Speleol. 38, 41–53.
Rossi, C., Lozano, R.P., Isanta, N., Hellstrom, J., 2010. Maganese stromatolites in caves: El Soplao (Cantabria, Spain). Geology 38, 1119–1122.
Sánchez-Navas, A., Martin-Algarra, A., 2001. Genesis of apatite in phosphate stromatolites. Eur. J. Mineralog. 13, 361–376.
Savarino, L., Stea, S., Granchi, D., Donati, M.E., Cervellati, M., Moroni, A., Pagantetto, G., Pizzoferrato, A., 1998. X-ray diffraction of bone at the interface with hydroxyapatite-coated versus uncoated metal implants. J. Mater. Sci. Mater. Med. 9, 109–115.
Schopf, J.W., Kudryavtsev, B.A., Czaja, A.D., Tripathi, A.B., 2007. Evidence of archean life: stromatolites and microfossils. Precambrian Res. 158, 141–155.
Schlyter, P., 2006. *Radiometry and photometry in astronomy FAQ* http://stjarnhimlen.se/comp/radfaq.html#10.
Seong-Joo, L., Browne, K.M., Golubic, S., 2000. On Stromatolite Lamination. In: Riding, R.E., Awramik, S.M. (Eds.), Microbial Sediments. Springer, pp. 16–24.
Sládecek, V., 1981. Indicator value of the genus Opercularia (Ciliata). Hydrobiologia 79, 229–232.
Smith, M., 2010. *Website of SEM images, accessed* 21–05–10 http://www.pbase.com/mattyjsmith/electron.
Soudry, D., 2000. Microbial phosphate sediment. In: Riding, R.E., Awramik, S.M. (Eds.), Microbial Sediments, pp. 127–136.
Stal, L.J., 2000. Cyanobacterial mats and stromatolites. In: Whitton, B.A., Potts, M. (Eds.), 2000. The Ecology of Cyanobacteria. Kluwer Academic Publishers, Dordrecht, Netherlands, pp. 60–120.
Stolz, J.F., 2000. Structure of Microbial Mats and Biofilms. In: Riding, R.E., Awramik, S.M. (Eds.), Microbial Sediments. Springer, pp. 1–8.
Taborõsi, D., 2006. Biologically influenced carbonate speleothems. Geol. Soc. Am. Spec. Pap. 404, 307–317.
Thimijan, R.W., Heins, R.D., 1982. Photometric, radiometric, and quantum light units of measure: a review of procedures for interconversion. Horticultural Sci. 18, 818–822.
Thurgate, M.E., 1996. The stromatolites of the cenote lakes of the lower south east of Australia. Helictite 34, 17–25.
Walter, M.R., 1976. *Stromatolites. Developments in Sedimentology*, 20. Elsevier, Amsterdam.
Wannier, M., 2009. Carbonate platforms in wedge-top basins: an example from the Gunung Mulu National Park, Northern Sarawak (Malaysia). Mar. Petrol. Geol. 26, 177–207.
Zürcher, S., Wäckerlin, D., Bethuel, Y., Malisova, B., Textor, M., Tosatti, S., Gademann, K., 2006. Biomimetic surface modifications based on the cyanobacterial iron chelator anachelin. J. Am. Chem. Soc. 128, 1064–1065.